Journal Pre-proof

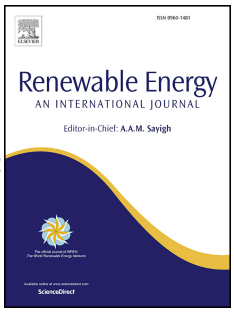

Influence of microalgae on synergism during co-pyrolysis with organic waste biomass: A thermogravimetric and kinetic analysis

Arun K. Vuppaladadiyam, Elsa Antunes, Farrukh Shehzad, Paula Blanco Sanchez, Hubao Duan, Ming Zhao

PII: S0960-1481(20)31780-8

DOI: https://doi.org/10.1016/j.renene.2020.11.039

Reference: RENE 14480

To appear in: *Renewable Energy*

Received Date: 2 March 2020

Revised Date: 28 June 2020

Accepted Date: 8 November 2020

Please cite this article as: Vuppaladadiyam AK, Antunes E, Shehzad F, Sanchez PB, Duan H, Zhao M, Influence of microalgae on synergism during co-pyrolysis with organic waste biomass: A thermogravimetric and kinetic analysis, *Renewable Energy*, https://doi.org/10.1016/j.renene.2020.11.039.

Authors Contributions

Dr Zhao Ming and Dr Huabo Duan are the Corresponding authors for the manuscript, who owns the leadership responsibility of the research activity, planning and execution.

Dr Arun K. Vuppaladadiyam and Dr Elsa Antunes conceived the idea and designed the experiments;

Arun K. Vuppaladadiyam performed the experiments;

Arun K. Vuppaladadiyam wrote the paper;

Dr Paula Blanco performed the data analysis and proof reading;

Influence of microalgae on synergism during co-pyrolysis with organic waste biomass: A thermogravimetric and kinetic analysis

Arun K. Vuppaladadiyam[1], Elsa Antunes[2], Paula Blanco Sanchez[3], Hubao Duan[1], Ming Zhao[4,5*]*

[1] School of Civil Engineering, Shenzhen University, 518000, China.

[2] College of Science & Engineering, James Cook University, Townsville, Queensland, 4811, Australia

[3] Chemical Engineering & Applied Chemistry, Aston University, B4 7ET Birmingham, United Kingdom

[4] School of Environment, Tsinghua University, Beijing 100084, China.

[5] Beijing Engineering Research Center of Biogas Centralized Utilization, Beijing 100084, China.

Corresponding Author *Email: ming.zhao@tsinghua.edu.cn (Ming Zhao)

Co-corresponding Author *Email: huabo@szu.edu.cn (Hubao Duan)

Graphical Abstract

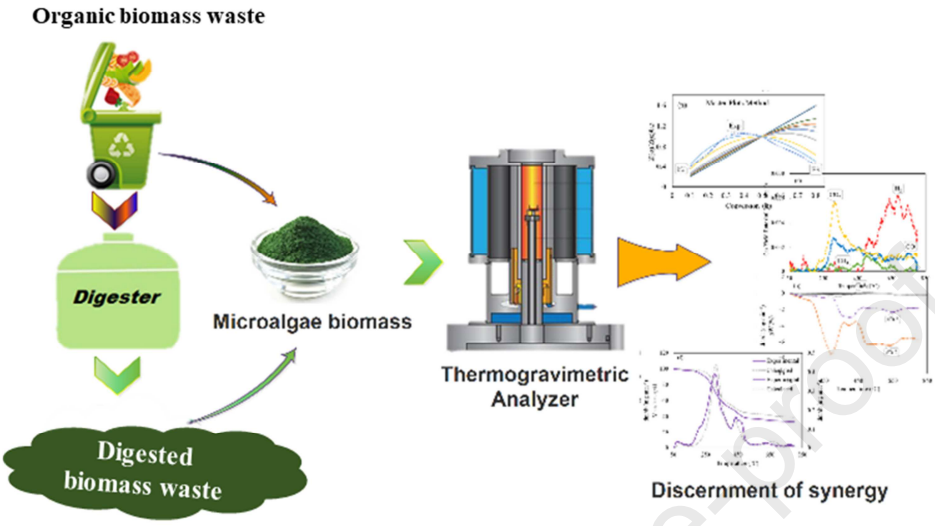

Influence of microalgae on synergism during co-pyrolysis with organic waste biomass: A thermogravimetric and kinetic analysis

Arun K. Vuppaladadiyam[1], Elsa Antunes[2], Farrukh Shehzad[3], Paula Blanco Sanchez[4], Hubao Duan[1], Ming Zhao[5,6*]*

[1] School of Civil Engineering, Shenzhen University, 518000, China.

[2] College of Science & Engineering, James Cook University, Townsville, Queensland, 4811, Australia

[3] Department of Chemical Engineering, King Fahd University of Petroleum & Minerals, Dhahran 31261, Saudi Arabia

[4] Chemical Engineering & Applied Chemistry, Aston University, B4 7ET Birmingham, United Kingdom

[5] School of Environment, Tsinghua University, Beijing 100084, China.

[6] Beijing Engineering Research Center of Biogas Centralized Utilization, Beijing 100084, China.

Corresponding Author *Email: ming.zhao@tsinghua.edu.cn (Ming Zhao)

Co-corresponding Author *Email: huabo@szu.edu.cn (Hubao Duan)

Abstract

The synergistic influence of microalgae on the two forms of organic waste biomasses, namely biomass wastes (BW) and its digested form (DBW), during co-pyrolysis was evaluated based on the thermal decomposition behaviour, gas yields, extent of thermal decomposition and reaction kinetics. The biomasses and their blends were co-pyrolysed at three different heating rates (10, 15 and 20 □C min^{-1}) in a thermogravimetric analyzer coupled with a mass spectrometer. Initial assessment, based on TG-DTG data, revealed that the thermal degradation can be divided into three zones (50-150 □C, 150-550 □C and 550-800 □C) for all the biomasses and their blends. The thermogravimetric data was used to evaluate the kinetic triplet, which include apparent activation energy (E_α), pre-exponential factor (A) and reaction mechanism, $f(\alpha)$. Semi-quantitative method was used to quantify the gas species, H_2, CO_2 and CO were dominant

species, implying the water gas reactions and oxidation reactions were predominant. The synergistic influence of microalgae was clearly evident in terms of reaction kinetics, as noted in the reduction in the apparent activation energy and increase in the total gas yields. The obtained kinetic triplet and thermodynamic parameters are expected to facilitate the design and optimization of co-pyrolysis of microalgae with other forms of organic wastes.

Keywords: Biomass, Co-pyrolysis, Thermogravimetric, Kinetic analysis, Microalgae.

1. Introduction

The global energy sector, till date, largely rely on fossil-based resources for energy production, resulting in serious environmental issues such as global warming. However, it is to be noted that at the current consumption rate, the fossil reserves are estimated to last not more than 50 years.[1] Owing to facts such as depletion of fossil fuels, rises in greenhouse gases emissions, the research in the last few decades has been directed to identify alternative energy resources [2]. Biofuels generated from sources like biomass are considered to be ideal substitutes to traditional fossil-based fuels and are extensively studied in the recent past [3-5]. Additionally, legislation of biofuels, in many developed countries, as renewable fuel standard and renewable portfolio standard has been done to promote their early adoption [6]. Alongside the advantages, the first generation biofuels (largely produced from edible crops) are reported to pose a range of issues such as rise in price of edible crops, water shortage and competition between food and fuel [7]. The second-generation biofuels, derived from lignocellulosic wastes, can address the issues associated with its forerunner; although, they still have limitations such as transportation of biomass, cost-intensive and pre-treatment [8].

The third-generation biofuels, produced from microalgae biomass, appear to be promising alternatives to its predecessors. Microalgae present many advantages over lignocellulosic biomass, such as higher conversion efficiency of incident light, higher lipid contents and exceptional growth rates, making them a sustainable feedstock for bioenergy based industry [9]. Additionally, a sustainable and carbon neutral mode of biofuels production can be made possible when the microalgae cultivation units are integrated with powerplants/cement industries and wastewater treatment units [10]. In addition to microalgae based biofuel production, domestic waste biomass, which contain materials such as paper, plastic food waste, textile and wood materials, has been widely considered as potential resource for sustainable energy production

and resource recovery [3]. China, which is the world most populated country, has produced *ca.* 179.36 million tons of domestic wastes in 2011 and the production is expected to increase to 480 million tons by 2030 [11].

Biochemical (anaerobic digestion) and thermochemical (pyrolysis) techniques are widely employed to convert biomass to bioenergy. However, either of them has their own advantages and limitations. During the anaerobic digestion (AD) process, some polymers such as Klason lignin are not effectively degraded and consequently gets accumulated in the digested residues, making it an ideal feedstock for the pyrolysis process, for example, in an integrated system [12]. There are, however, few drawbacks for pyrolysis, such as high oxygen and water content in the pyrolysis liquid products. These disadvantages can be eliminated by employing co-pyrolysis where the synergistic interaction between two feedstocks help compensate the drawbacks of one feedstock with the merits of other feedstock [5]. It is to be noted that the structural components of microalgae, which are lipids, proteins and carbohydrates, are completely different from the structural components of organic domestic wastes, which are cellulose, hemicellulose, lignin. Under such conditions, the mechanism of interactions between microalgae and domestic waste biomass or its digested form during thermal conversion is still unclear. Kinetic analysis could provide valuable information related to the rate and degree of reaction, which can help understanding the co-pyrolysis process [13]. The iso-conversional kinetics are highly recommended by the International Confederation for Thermal Analysis and Calorimetry (ICTAC) to derive meaningful kinetic data for a solid-state process [14, 15].

In the present study, the synergistic influence of microalgae, *Spirulina platensis* (SP) on domestic biomass waste (hereafter will be referred as biomass wastes, BW) and its digestate (hereafter will be referred as digested biomass wastes, DBW) has been evaluated based on the thermal behaviour, evolved gases and kinetic behaviour. *Spirulina platensis* has been widely investigated than most of the microalgae and is reportedly one of the frontrunners as a feedstock for biofuel production. Additionally, to the best of our knowledge, there is very limited research available on co-pyrolysis of microalgae with organic form of solid waste [5, 16]. Under such conditions, it is vitally important to understand the influence of an established microalgae on organic biomass waste during co-pyrolysis process. Three different mixing ratios (w/w), under each combination, were selected and were pyrolyzed under same conditions. The blends obtained from SP and BW were named as SB-1 (25% SP and 75% BW), SB-2 (50% SP and 50% BW) and SB-3 (75% SP

and 25% BW) and the blends obtained from SP and DBW were named as SD-1 (25% SP and 75% DBW), SD -2 (50% SP and 50% DBW) and SD -3 (75% SP and 25% DBW). Two iso-conversional methods, Kissinger-Akira-Sunnose (KAS) method and Friedman method, were used to obtain the apparent activation energy (E_α) and compensation effect was used to derive the pre-exponential factor (A) and reaction mechanism function, $f(\alpha)$. Furthermore, the reaction mechanism obtained using compensation effect was confirmed against the one obtained from generalised master plots method. Finally, the obtained kinetic triplet (E_α, A and $f(\alpha)$) was validated by comparing the experimental and simulated conversion vs temperature curves. The most common reaction mechanism functions studied and reported in the literature can be found in the Supplementary Information, Table S1.

2. Materials and Methods

2.1. Materials

Microalgae, *Spirulina platensis* (SP) was collected from Phycospectrum Environmental Research Centre (PERC), Chennai, Tamil Nadu, India. Using a suitable media, the microalgae was further cultivated in the lab under controlled conditions, with CFTRI media, temperature of 30°C and a light intensity of 500 lux. After the cultivation phase, the solid phase of the culture was separated from the liquid phase using a centrifuge at 6500 rpm for 15 min. The solid biomass was washed with deionized water and was dried in an oven at 80°C to obtain dry biomass. organic biowaste was synthetically prepared in the lab based on the available literature. Different fractions of BW, such as food waste, paper, textile, rubber and wood, were mixed according to their proportions in real organic biowaste [3]. BW was then digested in an Automatic Methane Potential Test System II (Bioprocess Control, Sweden) to completely digest the samples. The digestion process was run in triplicates, in 0.6 L reactors, to ensure the complete digestion. Growth characteristics of the microalgae and digestion characteristics of BW are out of the scope of the present study, therefore are not reported here. The proximate, ultimate, biochemical and structural analysis for the selected materials are presented in **Table 1** and the elemental analysis is presented in **Table 2**.

Table 1. Characterization the biomass samples.

Parameters	Sample	SP	BW	DBW
Proximate analysis (wt %)	Moisture	4.73	7.13	6.88
	VM	84.30	75.73	42.79

	FC	5.85	6.38	9.21
	Ash	5.14	16.75	47.61
Ultimate analysis (wt %)	C	47.02	55.67	31.83
	H	6.83	7.57	4.50
	O	27.81	33.99	60.53
	N	10.53	2.77	3.14
	S	0.82	0.43	0.78
Biochemical composition (wt %)	Carbohydrate	19.80	−	−
	Protein	62.60	−	−
	Lipid	8.70	−	−
Structural component analysis (wt %)	Lignin	−	7.38	17.67
	Cellulose	−	61.74	35.72
	Hemicellulose	−	12.42	29.49

Table 2. Heavy metal analysis of the selected samples.

Metal	Mg	Al	Si	P	S	Cl	K	Ca	Mn	Fe	Zn	Cu	Ni
SP (%)	19.30	0.72	0.59	33.6	8.46	2.52	21.6	1.62	0.25	0.50	0.01	0.01	0.01
BW (%)	3.41	0.78	2.76	5.5	1.78	6.83	14.4	21.70	0.03	1.06	0.13	0.01	0.07
DBW (%)	4.98	2.16	10.40	8.3	1.69	0.25	2.88	14.70	0.22	3.19	0.75	0.22	0.01

2.2. TG-DTG and evolved gas analyses

The thermogravimetric (TG) and derivative thermogravimetric (DTG) analysis of the selected samples (SB1-3, SD1-3) were carried out in a thermal analyzer (Q600), where *ca.* 6 mg of the sample was heated from ambient temperature to 800°C. Three different heating rates, 10, 15 and 20 °C min^{-1}, were used to analyse the thermal and kinetic behaviour of pure materials and their blends (SB1-3, SD1-3). Argon was used as purge gas at a flow rate of 500 mL min^{-1} to maintain and inert environment and assure accurate pyrolysis conditions within the system. The pyrolysis gas was delivered to a mass spectrometer (MS) via a heated capillary. The scanned ions and their respective gas species are presented in **Table 3**.

Table 3. Ion fragments and their representative gas species.

m/z	Ion fragments	Representative Species
2	H_2^+	Hydrogen
15	CH_4^+	Methane
28	CO^+	Carbon monoxide
40	Ar^+	Argon
44	CO_2^+	Carbon dioxide

Taking into consideration the weight of the biomass sample and Ar flow rate, the raw signals from MS were normalized using the below equation [ref];

Normalized signal for key molecule fragments 'i' = $(IC_i*500)/(IC_{Ar}*wt._{sample})$ (1)

where, IC_i and IC_{Ar} represents *m/z* signals for molecular ion fragments and Ar, respectively, 'i' represents arbitrary unit and $wt._{sample}$ is the biomass weight (g). A more detailed explanation of the procedure is mentioned in our previous study [17].

2.3. Kinetic analysis of co-pyrolysis of biomass and their blends

Pyrolysis of biomass varies with the type of biomass because the chemical structure of the all categories of biomass is not the same. However, the biomass pyrolysis pathway can be defined as biomass decomposition into char, volatiles and gases. According to Arrhenius fundamental equation, the rate constant $k(T)$ could be defined;

$$k(T) = Ae^{(\frac{-E_\alpha}{RT})} \quad (2)$$

where E_α and A represent apparent activation energy (J $mole^{-1}$) and pre-exponential (s^{-1}) of the reaction, respectively, and T and R represent absolute temperature (°K) and universal gas constant (8.314 J mol^{-1} K^{-1}), respectively.

The thermal decomposition of biomass is reflected by the degree of conversion (α) and can be defined as:

$$\alpha = \frac{m_0 - m_t}{m_0 - m_\infty} \quad (3)$$

where $m_{0,}$ reflects the initial mass, $m_{\infty,}$ reflects the final mass and m_t reflects the instantaneous masses during thermal conversion process.

The kinetics of a heterogeneous solid state reaction can be defined as [18]:

$$\frac{d\alpha}{dt} = k(T) f(\alpha) = Ae^{(\frac{-E_\alpha}{RT})} f(\alpha) \quad (4)$$

where, $f(\alpha)$ and t represents reaction mechanism function and time, respectively.

Taking the logarithm on both side of Eqn. (4) and rearranging terms generates Friedman equation [19]:

$$\ln\left(\frac{d\alpha}{dt}\right) = \ln\left[A(\alpha) f(\alpha)\right] - \frac{E_a(\alpha)}{RT} \quad (5)$$

The heating rate (β), since temperature is a function of time and increases with heating rate, can be defined as;

$$\beta = \frac{dT}{dt} = \frac{dT}{d\alpha} \times \frac{d\alpha}{dt} \quad (6)$$

Form the Eqns. (2) and (6),

$$\frac{d\alpha}{dT} = \frac{A}{\beta} e^{\left(\frac{-E_\alpha}{RT}\right)} f(\alpha) \quad (7)$$

The integrated form of f (α) is stated as follows;

$$g(\alpha) = \int_0^\alpha \frac{d\alpha}{f(\alpha)} = \frac{A}{\beta} \int_{T_0}^{T} e^{\left(\frac{-E_\alpha}{RT}\right)} dT \quad (8)$$

As Eqn. (8) does not have an exact solution, numerical methods or approximations are necessary to arrive at the final solution. Iso-conversional methods, taking into consideration their outstanding adaptability and validity, were considered to assess the apparent activation energy (E_α) of the pyrolysis process. Thus, one method from each category, differential (Friedman method) and integral (Kissinger-Akahira-Sunose) methods, were considered to obtain the E_α. Furthermore, the values of A and $f(\alpha)$ were obtained considering the E_α obtained from Friedman method.

The Kissinger-Akahira-Sunose (KAS) method is as follows [20]:

$$\ln\left(\frac{\beta}{T^2}\right) = \ln\left[\frac{AR}{E_\alpha\, g(\alpha)}\right] - \frac{E_\alpha}{RT} \quad (9)$$

By plotting $\ln(\beta/T^2)$ vs. 1/T for KAS method and ($\ln(d\alpha/dt)$ vs. 1/T for Friedman method and evaluating the slopes derived from the above plots, the apparent activation energy can be obtained for the conversion process.

2.3.1. Evaluation of pre-exponential factor and reaction mechanism

A strong linear relationship between the Arrhenius parameters, $\ln A_i$ and $E_{\alpha i}$, obtained under a single heating rate can be defined as compensation effect. As A_α is held together with $f(\alpha)$ in the evaluation function, using model-free methods such as Friedman or KAS methods, does not help evaluate the accurate values of A_α. However, compensation effect can be used to accurately evaluate the values of A_α [15, 21, 22]. By taking logarithm on both sides of Eqn. (4) and re-arranging the terms;

$$\ln\left[\frac{1}{f_i(\alpha)}\frac{d\alpha}{dt}\right] = \ln A_i(\alpha) - \frac{E_\alpha(\alpha)}{RT} \quad (10)$$

where, *i* refers to the mechanism function listed in Table S1. By substituting the mechanism functions listed in Table S1 into Eqn. (10) a pair of $\ln A_i$ and $E_{\alpha i}$ could be generated. The compensation equation can then be given by:

$$\ln A_i = a^* E_{\alpha i} + b^* \quad (11)$$

The values of a^* and b^* can be obtained by linear fitting different pairs of $\ln A_i$ and $E_{\alpha,i}$. Substituting the values E_α, obtained by using Friedman iso-conversional method, and a^* and b^* obtained from the above equation, the values of $A(\alpha)$ can be obtained from Eqn. (12),

$$\ln A_\alpha = a^* E_\alpha + b^* \quad (12)$$

The reaction mechanism function can be obtained by rearranging the terms in Eqn. (4) and is given as,

$$f(\alpha) = \left(\frac{d\alpha}{dt}\right)_\alpha \left[A_\alpha \exp\left(-\frac{E_\alpha}{RT}\right)\right]^{-1} \quad (13)$$

Substituting the values of A_α and E_α and using the experimental values of ($d\alpha/dt$) and T_α, in Eqn. (13), the mechanism function $f(\alpha)$ can be built numerically. All the mechanism functions listed in Table S1 fall under three categories, namely accelerating, decelerating or sigmoidal. The $f(\alpha)$ generated using compensation effect describes the nature of the reaction mechanism mentioned above. However, allowing to match experimental curves to theoretical curves, the master-plots method helps to exactly identify the mechanism function. In the present study, $Z(\alpha)$ master-plots method [23] was employed and by using the experimental values obtained for $d\alpha/dt$) and T_α the reaction mechanism can be obtained by using Eqn. (14):

$$\frac{Z(\alpha)}{Z(\alpha)_{0.5}} = \frac{f(\alpha)\,g(\alpha)}{f(\alpha)_{0.5}\,g(\alpha)_{0.5}} = (T/T_{0.5})^2 \left(d\alpha/dt\right)_\alpha \Big/ \left(d\alpha/dt\right)_{0.5} \quad (14)$$

where, 0.5 implies conversion at $\alpha = 0.5$.

The experimental and theoretical curves obtained from the right-hand side and middle terms of Eqn. (14), respectively, are matched against each other to identify the accurate reaction mechanism function.

The most important thermodynamic parameters, such as, enthalpy (ΔH), Gibbs free energy (ΔG), and change in entropy (ΔS), which are crucial in designing a reactor for the pyrolysis process were identified by using Eqns. (15) to (17) [4, 24]:

$$\Delta H = E_\alpha - RT \quad (15)$$

$$\Delta G = \mathrm{E}_{\alpha} + \mathrm{RT}_m \ln\left[\frac{k_B \mathrm{T}_m}{h A}\right] \quad (16)$$

$$\Delta S = \frac{\Delta H - \Delta G}{\mathrm{T}_m} \quad (17)$$

where, k_B, T_m and h are Boltzmann constant (1.381×10^{-23} J K^{-1}), DTG peak temperature and Plank constant (6.626×10^{-34} J s), respectively.

3. Results and Discussions

3.1. Influence of raw and digested organic biowastes on the thermal behavior during co-pyrolysis with microalgae

The thermogravimetric (TG) and derivative thermogravimetric (DTG) curves for biomasses and their blends obtained from SP and BW and SP and DBW at 15 °C min^{-1} are presented in **Fig. 1 (a) - (f)**, respectively. It should be noted that, during pyrolysis, the mass loss of the biomass is due to the release of vapours and gases. The DTG curves, shown in Fig. 1 (b), (d) and (f) can be characterised into three stages. During the first stage, in temperature region < 150 □C, there has been a minimal weight loss noticed with all the samples and is mainly due to dehydration [25]. The weight loss in this stage was approximately 1.04, 0.36, 0.72, 0.95, and 1.3% for SP, BW, SB-1, SB-2 and SB-3, respectively. The second stage is considered as the main pyrolysis stage, in the temperature range 150 – 600 □C, where the major weight loss has been noticed. The weight loss was noticed to be 67.12, 77.57, 73.7, 71.98 and 76.47% for SP, BW, SB-1, SB-2, and SB-3 samples, respectively. For SP, in stage II, a main peak followed by a lean shoulder can be noticed, where the main peak, at around 313 □C, can be attributed to the degradation of carbohydrates and proteins. As the lipids are known to degrade over a wide range of temperature, the shoulder at around 425 – 475 □C can be attributed to the degradation of lipids in the microalgae. It has been reported that the cracking, decarboxylation and depolymerization of carbohydrates, lipids and proteins, may happen in this temperature zone [26]. On the other hand, the DTG profile of BW in stage II can be characterised by a shoulder followed by three peaks at temperatures 211, 319, 379, and 438 °C. The shoulder on the left can be the degradation of hemicellulose and proteins, available in the wood and food portion of BW [27, 28]. The first peak can be attributed to the degradation of cellulose in wood and carbohydrates and proteins present in the food portion of BW [27, 28]. The second peak can be ascribed to the degradation

of rubber and/or paper wastes, as described in results reported in literature [29, 30]. The third peak corresponds to the degradation of plastic waste in BW [29, 31]. For DBW, from Fig. 1 (f) the percentage of weight loss happened during stage I (0-150°C), II (150-600°C) and III (600-800°C) were noticed to be 1.43, 44.38, and 5.94%, respectively. The weight loss for DBW in stage II was significantly lower than BW, which was 77%. The DTG profiles indicate a minor weight loss in stage I, mainly due to the dehydration [25]. In the stage II, two characteristic peaks were noticed at 339 and 430°C. Unlike BW, where three peaks were noticed in the stage II, the DTG curve have not showed the third peak at 379°C for DBW. The reason could be the degradation of paper waste occurred during the anaerobic digestion [32]. The first and second peaks in stage II for DBW could be attributed to the remains of cellulose and plastic waste, respectively [33]. Additionally, a tiny shoulder was noticed in the temperature range 440-460 °C, can be explained by further of degradation of lignin, which remained in DBW after anaerobic digestion [32].

For the blended samples obtained from SP and BW, the overall trends appear much close to the dominant biomass. For SB-1, which contain BW as major part, the DTG profile is much similar to BW, whereas SB-3, which contain SP as major part the DTG profile is much closer to SP biomass. However, residual fraction left after pyrolysis for all blends fall in between the fraction left for individual biomasses, similar results were noticed during co-pyrolysis of *Chlorella* and kitchen waste [16]. The DTG profiles for blends are characterized by two peaks, a shoulder followed by the first peak. The major weight loss peaks were noticed to be at temperatures 438, 311 and 310 °C for SB-1, SB-2 and SB-3, respectively. For the blended samples obtained from SP and DBW, SD-1, SD-2 and SD-3, residual fraction left after pyrolysis for all blends fall in between the fraction left for individual biomasses, SP and DBW. Similar results were noticed during co-pyrolysis of microalgae and textile dying sludge [34]. The final residual mass left for SD-1, SD-2 and SD-3 were 43.53, 33.4 and 32.76%, respectively. It should be noted that there is no much difference in the residue left at the end of the pyrolysis for SD-2 and SD-2 even though the composition of microalgae varied significantly. The blends obtained from SP and DBW, SD-1, SD-2 and SD-3, had the DTG profiles much similar to the dominant biomass of the blend. In the second stage (150-600 °C), two significant peaks were noticed for SD-1 and SD-2; however, one peak followed by a shoulder was noticed for SD-3. The mass loss rate was noticed to be higher for SD-3 followed by the SD-2 and SD-1. This could be because of the high volatile

matter present in SP [34] and the order of dominance of SP in the blends followed SD-3>SD-2>SD-1. Similar behavior was noticed in other studies [35, 36]. The peaks at 313, 311 and 313°C could represent the degradation of remaining carbohydrates and proteins after digestion. The peaks at 434, 443 and 443°C and the shoulder in the same temperature range for SD-1, SD-2 and SD-3, respectively could be due to the plastic wastes in DBW that remained after digestion. In the third stage, significant peaks at 676, 620 and 620°C were noticed for SD-1, SD-2 and SD-3, respectively. These peaks can be attributed to the decomposition of char and other inorganics such as….

It should be noted form Fig. 1 that the initial decomposition temperature of BW was lower than SP, indicating that the volatile matter in BW was easily decomposed than SP. As the microalgae contains carbohydrates, lipids and proteins as structural components, which are macromolecular compounds with a complex structure, they require more energy to break down the chemical bonds and consequently their decomposition started at relatively higher temperature than BW. Additionally, as SP biomass contain more volatile matter than BW and DBW (Table 1), the pyrolysis intensity (dm/dt) was noticed to be higher. It should also be noted that the increase in the proportion of SP in blends increased the pyrolysis intensity, indicating that the higher the content of SP, the higher is the reactivity of blends and faster the mass loss rate, corresponding to the results reported in the study on co-pyrolysis of microalgae and textile dye sludge [34]. Therefore, blending SP with BW or DBW could avoid the drawbacks of one another and improve pyrolysis performance.

Further, the mechanism of synergy can be understood as the digestion process initiates the decomposition of biomass, which can be observed by data available in Table 1 where the volatile matter in DBW is much lower than in BW. Another important aspect is the change in structural component analysis of BW and DBW presented in Table 1. DSMW has a much higher percentage of hemicellulose, which decomposes at lower temperatures range (220–315 °C) than cellulose (300–400 °C). The cellulose content in DBW is about 58% of the percentage in BW. Additionally, the high thermochemical reactivity of microalgae demonstrated in Fig. 1 and its high volatile matter content (84.30wt% - Table 1) shows that synergistic effects are expected in the simultaneous thermochemical decomposition with BW and DBW. Another important synergetic mechanism of reaction is the devolatilization of proteins, which are 62.6 wt % of biochemical composition of this microalgae. The devolatilization of proteins was positively

impacted by the decomposition of hemicellulose and cellulose present in BW and DBW. The devolatilization of carbohydrates in a temperature range (130–180 °C) could also enhance the thermal decomposition of hemicellulose. Also, the metals that are available in the ashes of DBW might have supported the enhancement of synergy between the microalgae and DBW samples. However, it is important to evaluate and characterize the pyrolytic products to further explain the potential reaction mechanisms.

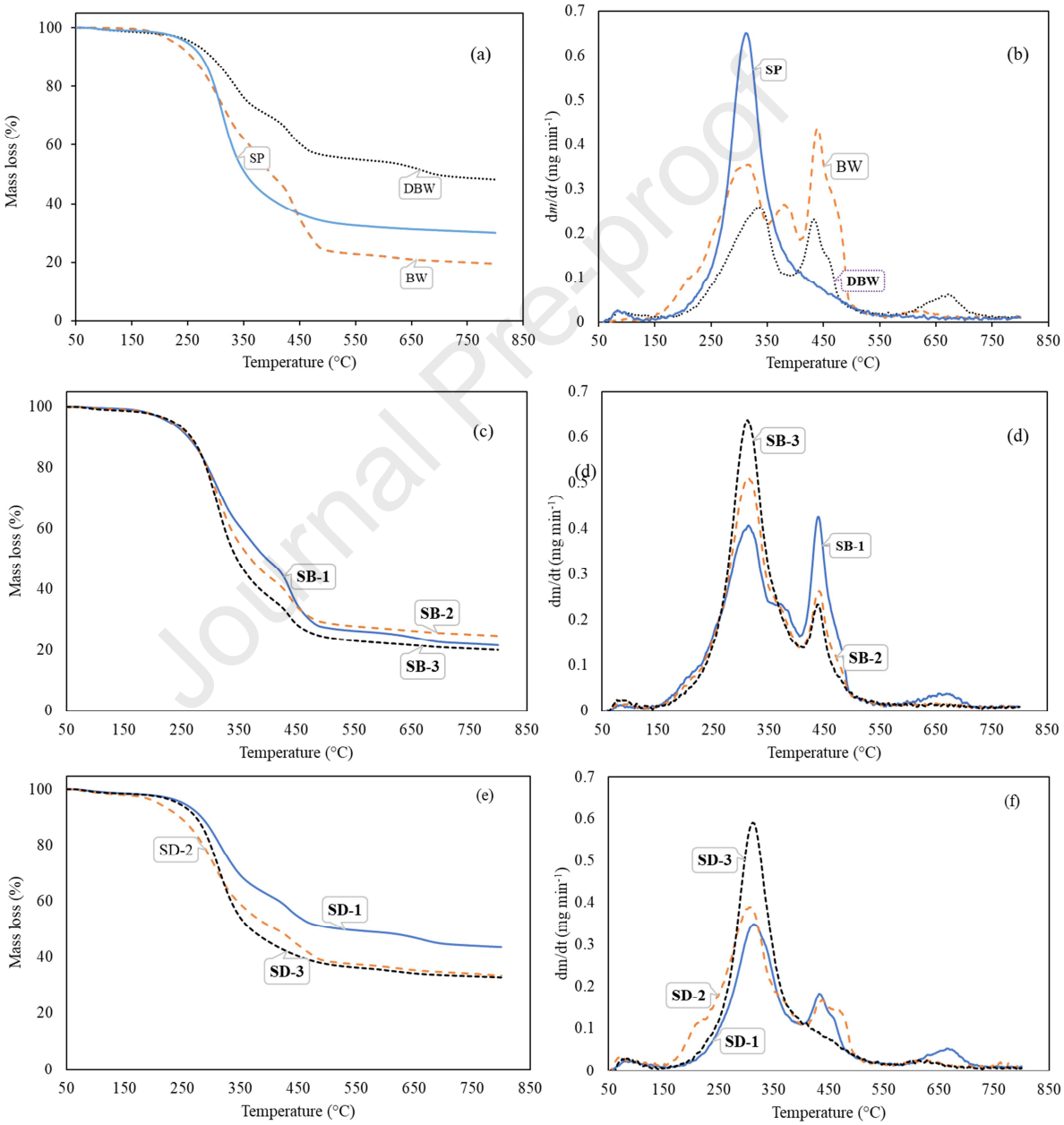

Fig. 1. Mass loss profiles at 15 °C min^{-1}, (a) TG for SP BW and DBW, (b) DTG for SP, BW and

DBW, (C) TG for SB-1, SB-2 and SB-3, (d) DTG for SB-1, SB-2 and SB-3 samples, (e) TG for SD-1, SD-2 and SD-3, (d) DTG for SD-1, SD-2 and SD-3 samples.

3.2. Influence of raw and digested organic biowastes on evolved gases during co-pyrolysis with microalgae

The evolved gas trends for all the samples SP, BW and DBW along with the blends of SP-BW and SP-DBW are presented in **Fig. 2 (a) - (k)**. For SP, BW, Fig. 2 (a) and (b), and their blends Fig. 2 (d)-(f), it is evident from that the evolution of gaseous components that co- pyrolysis occurred in two phases. In the first phase (200 – 400 °C), CO and CO_2 were the dominant gas species and in the second phase (400 -800 °C) H_2 was noticed to be dominant species for all the samples. The CO_2 evolution started at around 200 °C for plain samples and 150 °C for blends, whereas the CO evolution started a bit late, at around, 200-250 °C for samples and their blends. The evolution of CO and CO_2 was observed throughout the thermogravimetric run and were in accordance with major weight loss reported earlier. The possible reason for the evolution of CO_2 during the major weight loss stage could be because of the cracking and reforming of carboxyl (COOH) and carbonyl (C=O) groups [37]. One distinct peak was noticed for CO_2 for all the samples, during the major weight loss stage. It should be noted that, with blends, the evolution of CO_2 decreased sharply in the second phase (400 – 800 °C) with the increase in the proportion of SP. Similar results were reported during the co-pyrolysis of textile dying sludge and microalgae [34]. The evolution of CO, like CO_2, happened throughout the pyrolysis process. However, there were two peaks noticed for all the samples during the major weight loss stage, including blends. The formation of CO at temperatures < 400 °C could be mainly because of the by the cracking and reforming of thermolabile ether and carbonyl groups [38, 39]. On the other hand, CO released at temperatures >400 °C could be due to the secondary reactions related to char decomposition and scissions of diaryl ether groups [40]. There was a little CH_4 released during the pyrolysis process for all the samples and the plausible reason could be the cracking of methyl (−CH3) [41], methoxyl (−O−CH3) groups [40] and methylene ($-CH_2$) groups [39]. The release of H_2 started at temperatures above 450°C and continued till 800°C, which is in agreement with the literature reported [4, 24]. The reasons could be mainly tar cracking and reforming reactions. Additionally, the thermal decomposition of biomass enhanced by catalytic activity of alkali metal in the SP and BW ash, which further increased the yield of H_2 [42]. However, there was a mutual synergy noticed in the total gas yields, as reported in Fig. 2 (j). The total gas yields increased

with the increase in the proportion of SP in the blends. This could be mainly because of the high alkali metals in the ash of microalgae that would have enhanced the yield of gas via tar cracking and reforming reactions.

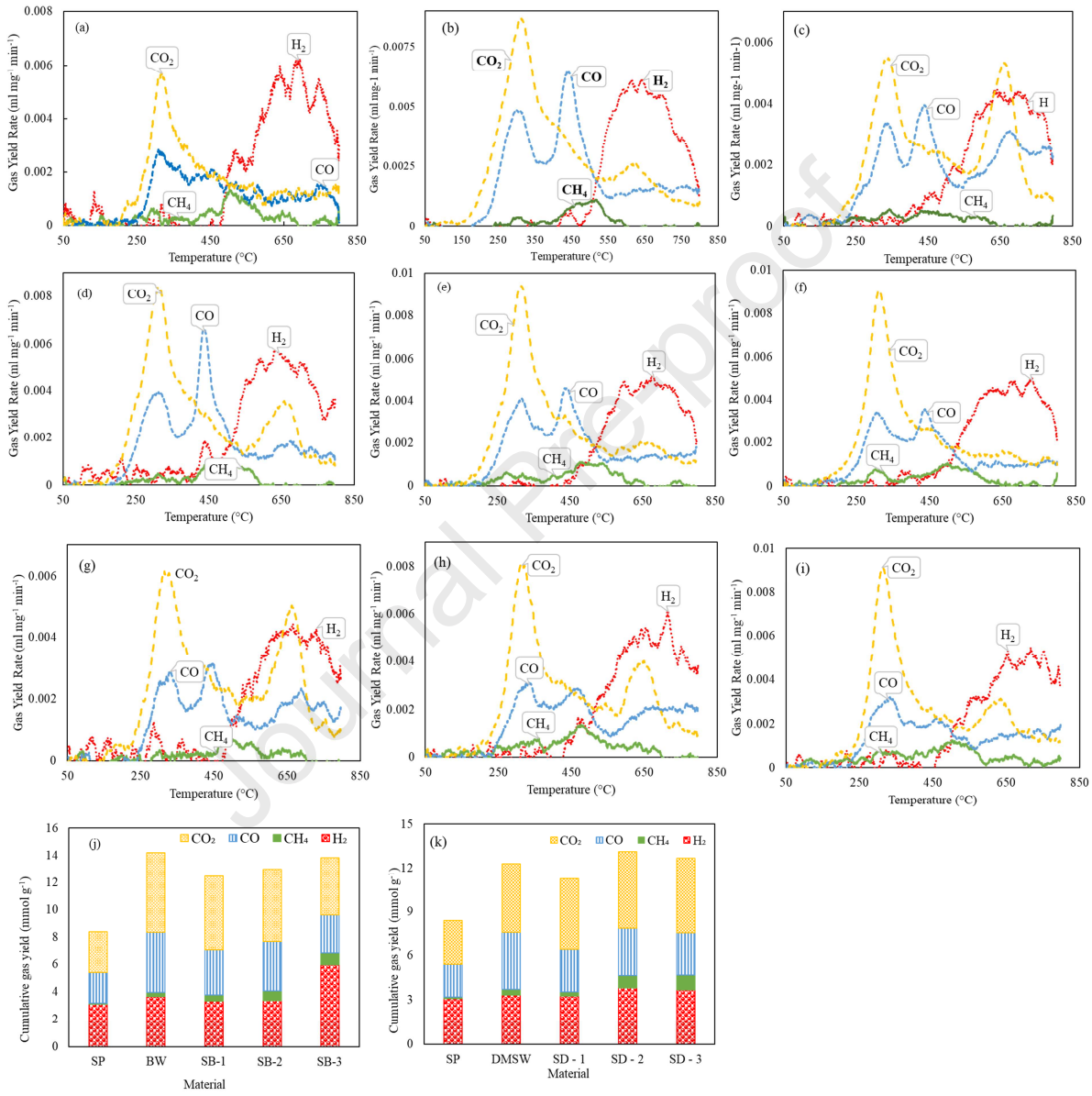

Fig. 2. Evolved gases for (a) SP, (b) BW, (c) DBW, (d) SB-1, (e) SB-2, (f) SB-3, (g) SD-1, (h) SD-2, (i) SD-3, (j) total gas yields for SP, BW and blends and (k) total gas yields for SP, DBW and blends.

For SP and DBW blends, Fig. 2 (g)-(i), two distinct phases of gas evolution were noticed for all the samples including blends. In the first phase (150-400°C) CO and CO_2 were noticed to be the

predominant gas species. As the temperature was further increased, H_2 started getting evolved and accompanying CO and CO_2. The evolution of CO and CO_2 occurred throughout the experiment. It is to be noted that the increase in temperature increased the reactivity and conversion of feedstock into gaseous products [43]. Furthermore, it is advisable to increase the temperature over 600°C to produce more burnable gases from microalgae biomass [44]. The evolution of CO started at around 250°C for all the samples and continued till the end of the run (800°C). The CO_2 evolution peaks for SP, DBW, SD-1, SD-2 and SD-3 were noticed to be 318, 338, 318, 315 and 312°C, respectively. It should be noted that the CO_2 yields decreased with the increase in the DBW proportion in the blend. Similar results were noticed during the co-pyrolysis of microalgae and plastic [45]. However, a second peak for CO_2 was noticed at around 640-670°C for all the samples except for SP. The possible reason could be the decomposition of calcium carbonate used as a filler on paper, which may be left undigested [46]. This is in good agreement with the results reported for weight loss, discussed above. The possible reason for the evolution of CO_2 during the major weight loss stage could be because of cracking and reforming of carboxyl (COOH) and carbonyl (C=O) groups [37]. In this case CO_2 and CO evolution was noticed all through the run till 800 °C. However, unlike CO_2, there were two distinct CO evolution peaks noticed for all the samples in the major pyrolysis zone (150-600°C). Additionally, there was a significant peak noticed in the third stage (600-800°C). The CO evolution in both, first and second stages can be attributed to the decomposition of volatiles and activation of Boudouard reaction, respectively [47]. The evolution of H_2 started form 400°C and continued till 800°C for all the samples which is in agreement with the literature [4, 24]. Additionally, the thermal decomposition of biomass enhanced by catalytic activity of alkali metal in the SP and DBW ash, which further increased the yield of H_2 [42]. The CH_4 evolution started at around 200°C and continued till 800°C. The plausible reason could be cracking of methyl (−CH3) [41], methoxyl (−O−CH3) groups [40] and methylene ($-CH_2$) groups [39]. However, there was significant synergistic effect noticed in the total gas yields presented in Fig. 2 (i) and (k). The total gas yields were high for SD-2 followed by SD-3 and SD-1.

3.3. Evaluation of synergy in the rate and extent of thermal decomposition during the co-pyrolysis of microalgae with raw and digested organic biowastes

To evaluate synergistic influence of microalgae on BW and DBW and vice-versa during the co-pyrolysis process, the experimental results (TGA data) were compared with the calculated

results. The calculated values for biomass pyrolysis are obtained using weighted additive model, which indicates the values obtained if the biomass samples were pyrolysed independently. This indicates a scenario where there is no synergistic interaction between the two samples and the calculated values are the sum of individual values corresponding to their mass ratio [16, 42]. Using Eqn. (18) and (19) [ref], the theoretical conversions of biomass blends are compared with the experimental data and the results are presented in **Fig. 3 (a) – (h).**

$$\alpha_{cal} = (1 - f_{MA})\alpha_{OSW} + f_{MA}\,\alpha_{MA} \quad (18)$$

$$\Delta W = W_{EXP} - W_{CAL} \quad (19)$$

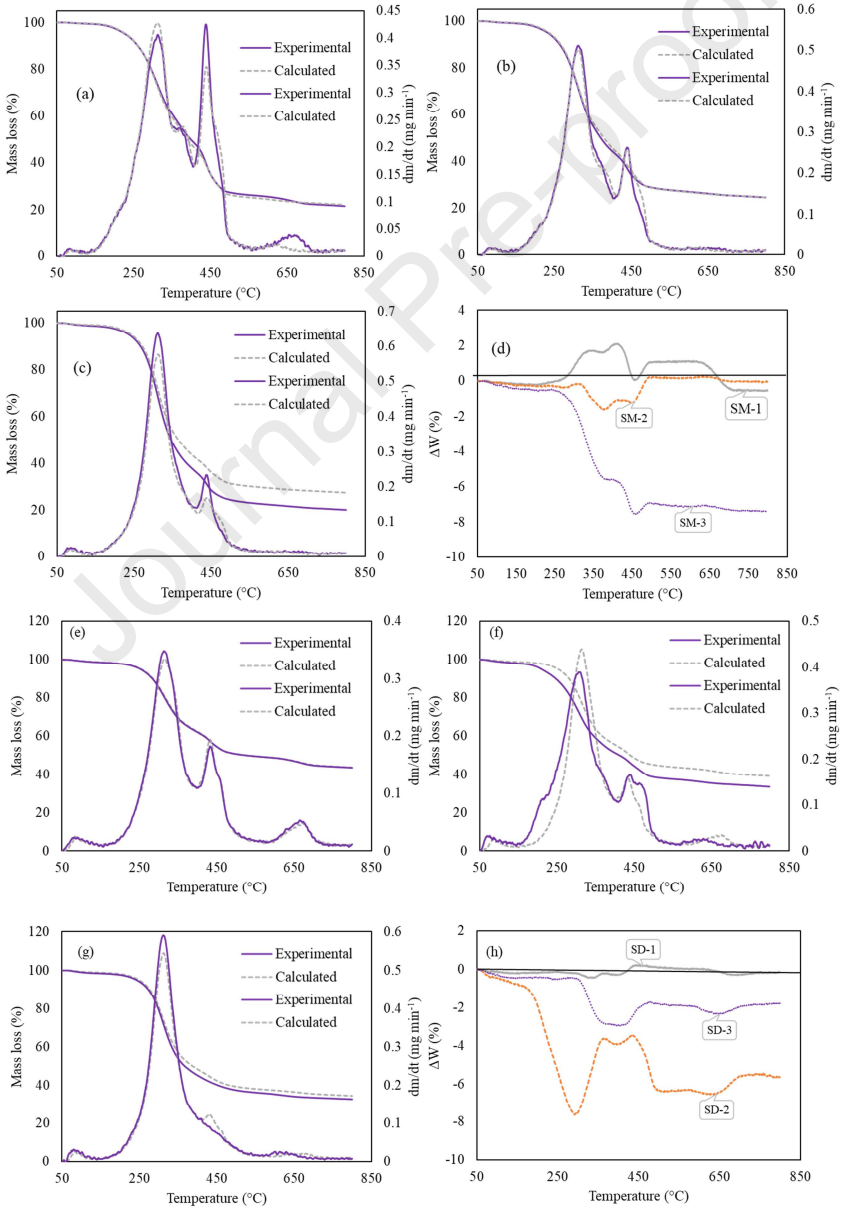

Fig. 3. Comparison of experimental and calculated TG and DTG profiles for biomass blends at the heating rate of 15 °C min^{-1}, (a) SB – 1, (b) SB – 2, (c) SB – 3 and (d) ΔTG curves, (e) SD – 1, (f) SD – 2, (g) SD – 3 and (h) ΔTG curves.

Fig. 3 demonstrates that the experimental and calculated TG and DTG profiles for SB-1 and SB-2 overlapped each other over most part of the conversion, indicating no possible synergy in either conditions. However, there is a tiny discrepancy noticed for SB-2 in the temperature range of 300-500°C, but the synergistic effect needs to be further clarified. The ΔTG values, as shown in Fig. 3 (d), indicate a clear positive value for SB-1, which explains it possessed an antagonistic effect. As it can be noticed from Fig. 3 (b) the tiny discrepancy is further justified by the negative values displayed for SB-2 in Fig. 3 (d). In the region of temperatures between 300 – 800°C, a significant disagreement was noticed between the calculated and experimental profiles of SB-3, which was further justified in Fig. 3 (d) with intense negative values for ΔW. Among the blends obtained from SP and BW, SB-3 has a higher thermal degradation than the other two blends, SB-1 and SB-2, corresponding the mutual synergy between the two biomasses during thermal degradation and is discussed in greater details in the subsequent sections. For blends obtained from SP and DBW, from the Fig. 3, the experimental and calculated TG and DTG profiles for SD-1 overlapped each other over most part of the conversion, indicating no possible synergy in such condition. However, there is a significant discrepancy noticed for SD-2 and SD-3 in the temperature range of 300-800 °C. The experimental values of thermal degradation for blends SD-2 and SD-3 were more intense than the calculated thermal degradation values of individual biomasses with same mass ratio, corresponding the mutual synergy between the two biomasses during co-pyrolysis and is discussed in detailed in the subsequent sections.

3.4. Kinetic analysis to evaluate the impact of microalgae on raw and digested BW and vice-versa

Thermogravimetric data, at three heating rates 10, 15 and 20°C min^{-1}, was used to evaluate the kinetic parameters for plain biomass samples and their blends. Chemical kinetics along with the depiction of transport process are important for the design and optimization of thermochemical conversion systems. Two iso-conversional methods, Friedman method (FM) and Kissenger-Akira-Sunnose (KAS) methods were used to estimate the activation energy for the pyrolysis of samples and their blends. Using Eqns. (5) and (9) the apparent activation energy (E_α) was

calculated over a selected range of conversion from 0.1-0.8, with a step interval of 0.5 and are presented in the supplementary information **Table S1**. Additionally, the average values of E_α, A, and other important thermodynamic parameters are presented in **Table 4.** The variation of activation energy, derived based on FM and KAS methods, with respect to conversion is presented in **Fig. 4 (a)-(f)**.

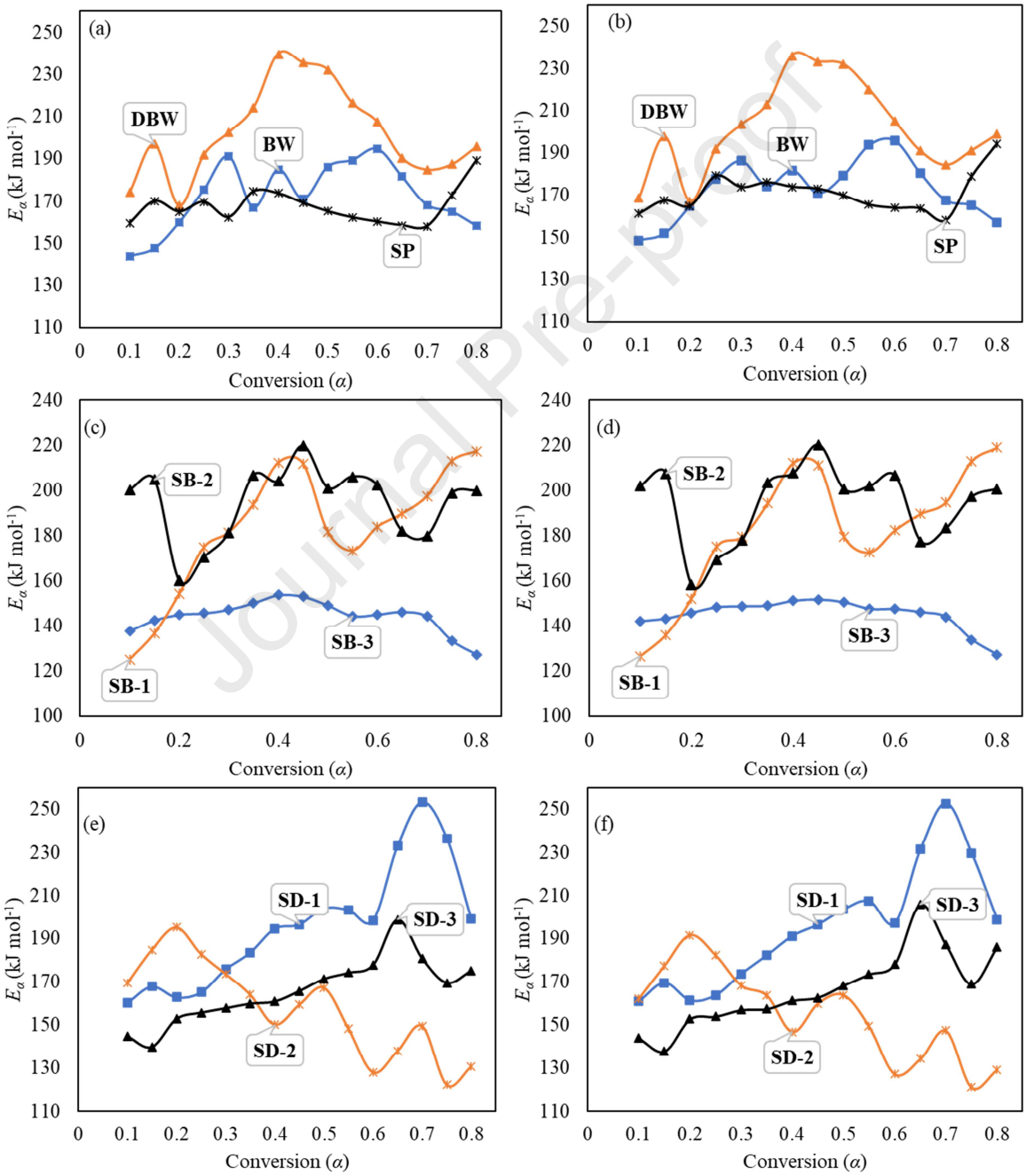

Fig. 4. Variation in activation energy with conversion for (a) FM, (b) KAS for SP, BW and DBW, (c) FM and (d) KAS for SB-1, SB-2 and SB-3, (e) FM and (f) KAS for SD-1, SD-2 and SD-3 biomass samples.

Activation energy can be defined as the minimum energy that is necessary to start a reaction, implying that the reaction with higher activation energy either need longer residence time or higher reaction temperature to gain sufficient energy to start the reaction [48]. Fig. 4 shows that the E_α is highly dependent on conversion, indicating the complex nature of biomass pyrolysis [49]. In general, as a result of parallel reaction routes wherein each route has a different activation energy, the activation energy increased with an increase in temperature to a certain conversion and then decreased. At the initial stages of conversion, the activation energy exhibited an increasing trend for two biomass samples and their blends. Subsequently, fluctuations in the trends of activation energy were noticed till the end of the process, which can be attributed to the complex reaction schemes mainly parallel complex reactions [50]. The lowest activation energy, on the basis of Friedman method, that is required to initiate the reaction was determined to be 159.65, 144.07, 174.41, 125.09, 200.04, 137.73, 160.04, 169.12 and 144.87 kJ mol^{-1} for SP, BW, DBW, SB-1, SB-2, SB-3, SD-1, SD-2 and SD-3, respectively. On the other hand, the average activation energy for the process was estimated to be 167.4, 172.3, 202.6, 182.92, 194.35, 144.36, 195.55, 157.45 and 165.50 kJ mol^{-1} for SP, BW, DBW, SB-1, SB-2, SB-3, SD-1, SD-2 and SD-3, respectively. Similar results were reported in the literature for the pyrolysis of similar feedstocks, for instance, for microalgae *Dunaliella tertiolecta* [51] and *Nannochloropsis oculata* [52], for MSW [31] and co-pyrolysis of MSW with other wastes [36, 53, 54]. The activation energy was high at lower conversion rates for the biomasses and their blends, indicating the initiation of pyrolysis of structural components such as lipids, proteins and carbohydrates and cellulose, hemicellulose and lignin in SP, BW and DBW, respectively. There was no clear trend noticed for plain biomass samples, but for blends the pyrolysis conversion can be divided into three stages.

The highest E_α values for SB-1, SB-2 and SB-3 were noticed to be 217.20 kJ mol^{-1} at α= 0.8, 220.13 kJ mol^{-1} at α=0.45 and 153.65 kJ mol^{-1} at α=0.4, respectively. The temperatures corresponding to the conversions having high activation energies were estimated to be 430°C (at α= 0.8) for SB-1, 325°C (at α=0.45) SB-2 and 320 and 350°C (at α=0.4) for SB-3. These

temperatures are in good agreement with the DTG peaks discussed earlier. The peak value E_α for SD-1, SD-2 and SD-3 were 253.2 kJ mol^{-1} (at α=0.7), 195.15 kJ mol^{-1} (at α=0.2) and 198.83 kJ mol^{-1} (at α=0.65), respectively. The average E_α values varied were in the range of 194.64-195.55, 154.89-157.65 and 165.6-166.25 SD-1, SD-2 and SD-3, respectively. The average E_α values for all the biomasses and their blends obtained in this study are in agreement with the studies reported in literature for microalgae [55, 56], organic solid wastes [51] and co-pyrolysis of similar feedstocks [16, 45, 57, 58]. The calculated average activation energies reported in Table 4 indicate that there has been a significant synergistic effect occurred in between the two biomasses in the blend SB-2, the calculated activation energy was much higher than the experimentally derived activation energy. In the other two cases, the calculated activation energy was lower than the experimental activation energy, indicating no possible synergy in blends SB-1 and SB-2. The calculated E_α value of blends SD-2 and SD-3 (Table 4) were noticed to be higher than the experimental E_α values, indicating synergistic interactions between both the feedstocks. The possible reasons for the synergistic effects could be the that the volatiles and extractives present in the SP biomass may have enhanced the degradation of the structural components in BW and DBW biomasses. The additional heating promoted by the volatile contents, present in the biomasses, may have improved the degradation during the pyrolysis process [42]. Furthermore, microalgae ashes are reported to have high alkali metal contents, which could have played the role of catalyst in enhancing the decomposition [59]. The variation in the activation energy with respect to the temperature is presented for the plain biomass sampes and their blends is shown in **Fig. 5.**

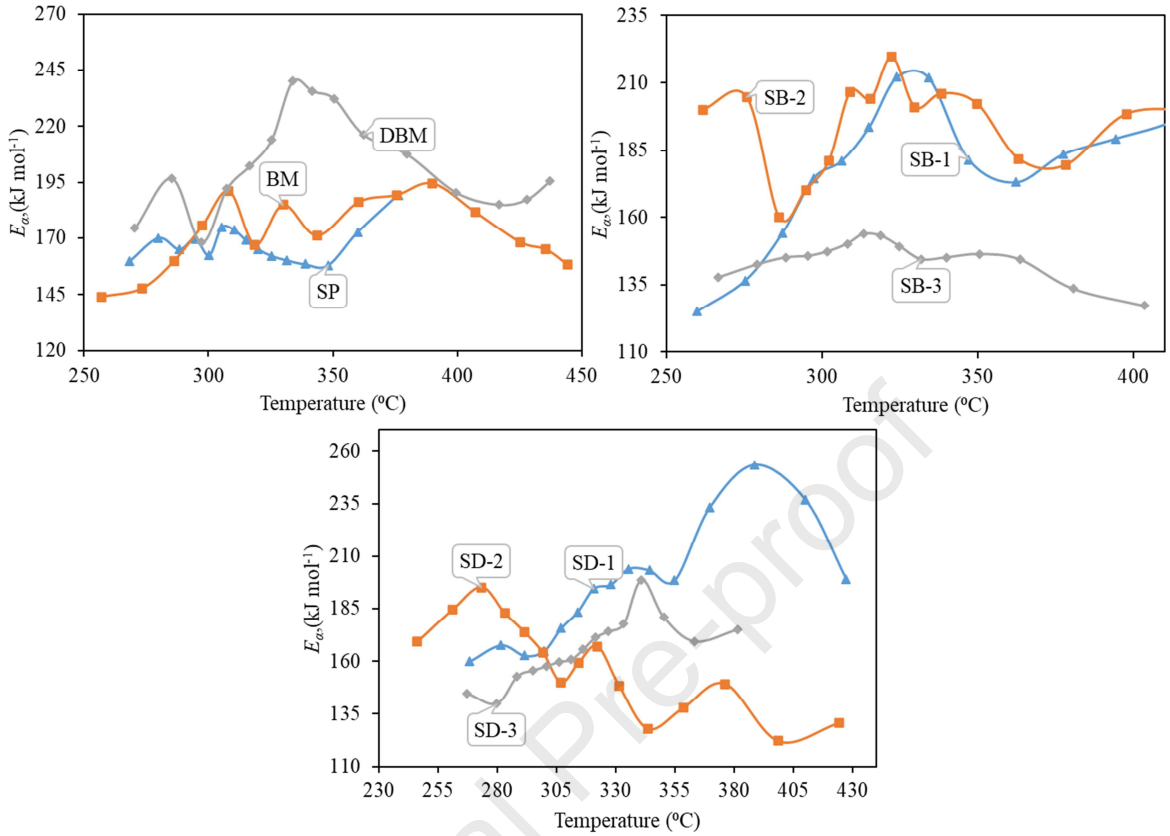

Fig. 5. Variation in the activation energy with respect to temperature for biomass samples.

It should be noted that the actiation energy for all the samples is in agreement with the discussion done in Section 3.1. It is to be noted that the activation energy was high for all the sampels corresponding to the DTG peaks shown in theie blends is Fig. 1. According to the literature, the activation energies required for the thermal decomposition of proteins, lipids and carbohydrates are the range of 20-220, 200-220 and 40-220 kJ mol-1, respectively and for cellulose, hemicellulose and lignin the activation energies were reported in the range of 128-263, 90-165 and 20-100 kJ mol^{-1}, respectively [60]. The activation energies and corresponding temperatures obtained int his study are in agreement with the literature.

Table 4. Average values of activation energy, pre-exponential factor, and other thermodynamic parameters for selected biomass materials.

Parameter	Activation Energy (E_α) Friedman method		Activation Energy (E_α) KAS method		Pre-exponential factor, *A*,	Enthalpy, ΔH,	Gibbs free energy, ΔG,	Entropy, ΔS,
Units	Average (kJ mol^{-1})	Calculated	Average (kJ mol^{-1})	Calculated	Average (s^{-1})	Average (kJ mol^{-1})	Average (kJ mol^{-1})	Average (J mol^{-1})

SP	167.4	–	170.93	–	2.29×10^{13}	162.48	169.58	-22.47
BW	172.3	–	173.02	–	1.81×10^{10}	167.12	173.04	-13.5
DBW	202.55	–	202.21	–	1.04×10^{18}	197.37	184.94	36.68
SB-1	182.92	171.07	182.43	172.5	4.45×10^{16}	177.89	171.87	13.75
SB-2	194.35	169.85	194.15	171.99	8.66×10^{16}	189.34	177.67	37.52
SB-3	144.36	168.63	145.17	171.45	8.57×10^{10}	139.39	157.31	-57.78
SD-1	195.55	193.76	194.63	193.39	4.13×10^{15}	190.49	191.89	-4.48
SD-2	157.45	184.97	154.89	186.57	3.73×10^{14}	152.47	161.82	-30.07
SD-3	165.6	176.19	166.25	178.75	3.75×10^{14}	160.68	166.7	-19.25

The compensation effect was used to evaluate the pre-exponential factor (*A*) values and other thermodynamic paramters were calculated by using Eqns. (15)-(17), are presented in **Table S4-S6**. The avarage valuse of *A* (s^{-1}) and thermodynamic parameters are presented in Table 4. To avoid the error associated with the integral methods [61], the activation energy values obtained by using Friedman differential method were used to obtain accurate values of pre-exponential factor, thermodynamic parameters and reaction mechanism function.

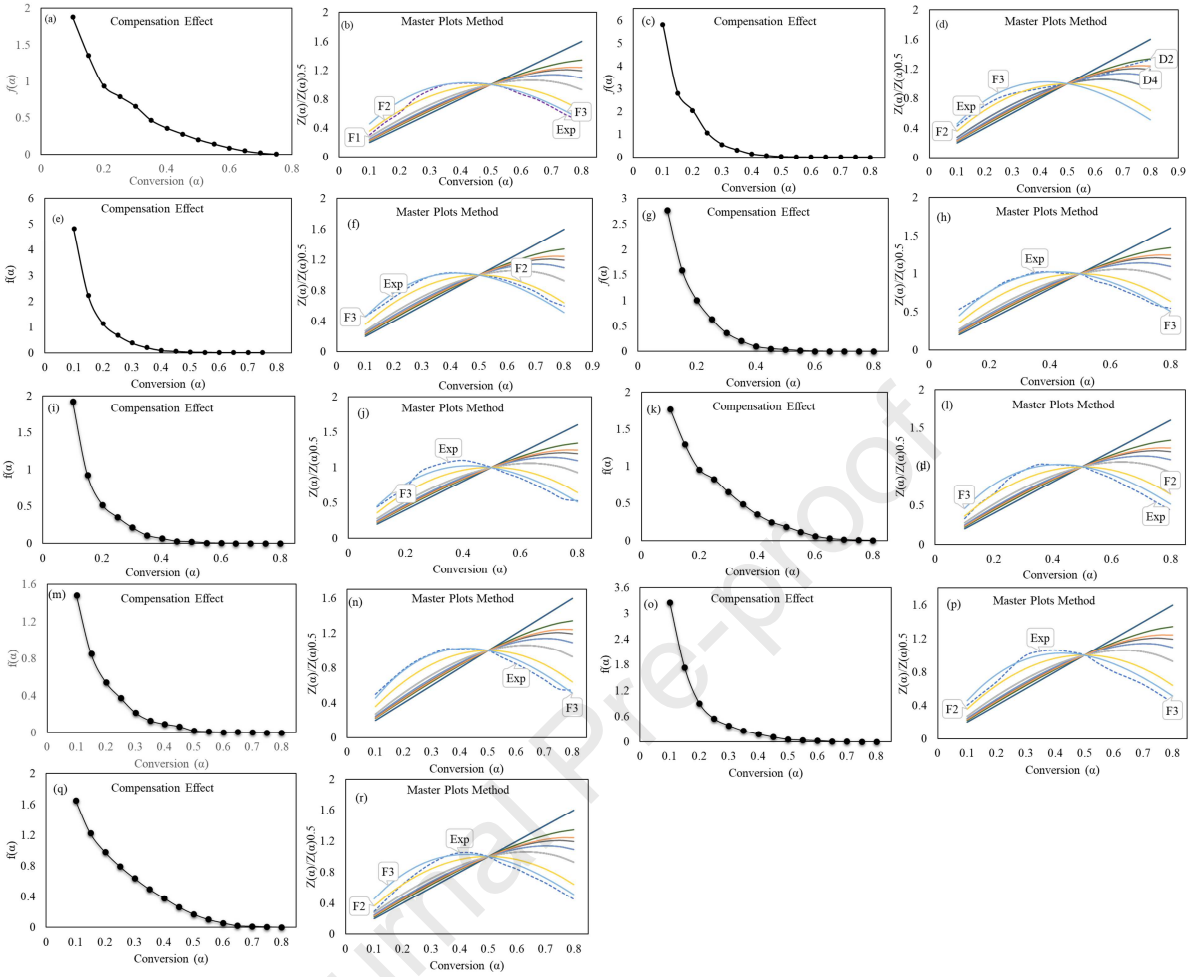

Fig. 6. Reaction mechanism function for (a), (b) SP, (c), (d) BW, (e), (f) DBW, (g), (h) SB-1, (i), (j) SB-2, (k), (l) SB-3, (m), (n) SD-1, (o), (p) SD-2 and (q), (r) SD-3.

By selecting different $f_i(\alpha)$, presented in Table S1, and using Eqn. (10), a pair of ln Ai and E_i were calculated and are presented in **Fig. S1.** Substituting the values of E_α obtained by using Friedman iso-conversional method in the Eqns. (11)-(12) yields the values of A, as shown in Table S4-S6. The values of A for all the samples varied from 10^{11} to 10^{14} for SP, 10^{10} to 10^{14} for BW, 10^{8} to 10^{17} for SB-1, 10^{12} to 10^{18} for SB-2 and 10^{9} to 10^{11} for SB-3. The average A values for SP, BW, DBW, SB-1, SB-2, SB-3, SD-1, SD-2 and SD-3 were noticed to be 2.29×10^{13}, 1.81×10^{10}, 1.04×10^{18}, 4.45×10^{16}, 8.66×10^{16}, 8.57×10^{10}, 4.13×10^{15}, 3.73×10^{14}, 3.75×10^{14}, respectively. The A values $\leq 10^{9}$ s^{-1} indicate surface reaction and if the reaction does not depend on the surface area the low values of A indicate the formation of tight junctional complex. On the other hand, the values of A over 10^{9} s^{-1} imply a loose junctional complex [62, 63]. The values of A fluctuating in

between $10^{10} – 10^{12}$ s^{-1} imply that the activated complex formed from the reagents is restricted in rotation [3]. The reaction mechanism function for all the biomass samples and their blends are presented in **Fig. 6 (a)-(r).** The reaction mechanism function generally categorized in to three categories, namely accelerating, decelerating and sigmoidal forms [21]. The overall trend of $f(\alpha)$ derived by using compensation effect for all the samples was monotonous function decreasing with respect to conversion, which are categorized under decelerating models, which is similar to pyrolysis of similar feedstocks [61, 64-66]. The trends observed in the present study fall under the category of decelerating models, such as reaction order or diffusion models.

While the mechanism function obtained by using compensation effect helps to identify the reaction mechanism type, master plots method helps to match the experimental reaction mechanism function to the available theoretical mechanism function and accurately identify the $f(\alpha)$ for a particular biomass under specified conditions. The generalized master plots strictly depend on the kinetic model used to fit the reaction and does not depend on the heating rate. Therefore, the master plots obtained under different heating rated should take similar shape [4]. The experimental and theoretical plots were obtained by using the right-hand side and left-hand side of Eqn. (14) and were plotted against conversion, as shown in Fig. 6. The experimental plots of SP closely matched with second order reaction model (F2) at lower conversions ($\alpha \leq 0.2$) and then shifted to third order reaction model (F3) at $\alpha > 0.2$. For BW the experimental plots matched with F3 model for $\alpha \leq 0.45$ and then shifted to second order diffusion model (D2) for $\alpha > 0.5$. Unlike BW which had the experimental plots matched with F3 model for $\alpha \leq 0.45$ and then shifted to second order diffusion model (D2) for $\alpha > 0.5$, the experimental plots of DBW matched with third order reaction model (F3) throughout the conversion range. The reason in the change of reaction mechanism of DBW as compared to the BW could be the influence of anaerobic digestion on the organic matter in the BW. The experimental plots for SB-1 and SB-2 closely matched with F3 reaction model for the whole process. However, the experimental plots of SB-3 were much similar to SP, were in close match with F2 at lower conversion ($\alpha \leq 0.2$) and shifted to F3 at $\alpha > 0.25$. The experimental plots for SD-1 closely matched with F3 reaction model for the whole process. However, the experimental plots of SD-2 and SD-3 were close match to F2 at lower conversion ($\alpha \leq 0.2$) and shifted to F3 at $\alpha > 0.25$.

The master plots indicates that the degradation process closely resembles the n^{th} order (random nucleation model). To find out the exact parameters, model fitting (nonlinear least square) was

carried out for the experimental data and the general model. Since, the process is multistep, first of all the dα/dt was deconvoluted into distinct peaks using Fraser–Suzukifunctionas it provided the best fit amongst other sigmoidal functions.. The model fitting was carried out for each stage (Stage 1, Stage 2 and Stage 3 (in some samples)) using MATHEMATICA© command "Non-Linear Model Fit" and the reaction order was calculated. All the models (general solid-state model) were checked and as expected the best fit was found for n^{th} order mechanism. The results are listed in **Table 5**.

Table 5. Reaction order of biomass pyrolysis process.

Sample	Stage 1		Stage 2		Stage 3	
	Reaction order (n)	R^2	Reaction order (n)	R^2	Reaction order (n)	R^2
SP	2.34	0.994	1.41	0.999	-	-
BW	1.52	0.999	1.73	0.994	1.12	0.973
DBW	1.34	0.999	1.81	0.997	-	-
SB-1	1.47	0.999	1.38	0.987	1.6	0.999
SB-2	1.65	0.999	1.73	0.994	2.13	0.999
SB-3	2.03	0.998	1.58	0.995	-	-
SD-1	1.6	0.999	1.61	0.999	-	-
SD-2	1.66	0.998	1.36	0.999	-	-
SD-3	1.72	0.999	1.89	0.997	-	-

The average values of thermodynamic parameters such, as activation enthalpy (Δ*H*), Gibbs free energy (Δ*G*) and activation entropy (Δ*S*), for the plain samples and blends are listed in Table 4 and detailed values are provided in Table S4-S6. From Tables S4-S6, it is evident that the energy difference between activated complex and reagent is in agreement with the activation energy. The small energy difference between E_α and Δ*H* indicate favorable conditions for the formation of activated complex. From the Tables 3, S4-S6, a small energy barrier of ~5 kJ mol^{-1} between E_α and Δ*H* indicate favorable conditions for the reaction to happen. The average Δ*H* values were noticed to be 162.48, 167.21, 197.37, 177.89, 189.34, 139.39, 190.49, 152.47 and 160.68 kJ mol^{-1} for SP, BW, DBW, SB-1, SB-2, SB-3, SD-1, SD-2 and SD-3, respectively. The average Δ*H* value was low for SB-3 under SM blends and for SD-2 under SD blends, indicating the requirement of low energy to break the bonds among the reactants. The change in Gibbs free energy (Δ*G*), imply the increase in the total energy of the system in the process of formation of activated complex. The high Δ*G* values indicate unfavorable conditions for the reaction to happen, as high energy is required in such conditions [67]. Furthermore, activation entropy indicates the degree of disorder of a reaction system. In case of pyrolysis, Δ*S* values imply the degree of alignment of carbon atoms in biochar. Also, the positive values of Δ*S* indicate that the

system is far from thermal equilibrium products and attainment of thermal equilibrium. While the positive values of ΔS indicate little reactivity and demands an increase in the reaction time to form activated complex, the negative values of ΔS indicate high reactivity and necessitates low reaction time to form activated complex. Additionally, it should be noted that the negative values of ΔS and the values of ΔH lower the ΔG, indicating that a significant proportion of heat supplied to system is unused [42].

Conclusions

The present study attempted to investigate the synergistic influence of microalgae on raw and digested forms of organic biowastes during co-pyrolysis process. The TG-DTG profiles of plain and blended samples showed three devolatilization with characteristic peaks and shoulders depending on the biomass and its ratio. The synergistic influence was not prominent; however, there was a change in the decomposition pattern during the co-pyrolysis process for all the blends. The volatiles and extractives in the microalgae biomass and the mineral contents in the ashes of the three biomass samples significantly enhanced the kinetics of the thermal decomposition process. The higher activation ΔG indicate the favourability of the raction to occur. Additionally, it should be noted that the impact of microalgae was different in different scenarios. A decrease in the values of activation energy and an increase in the gas yields were noticed with the increase in the proportion of microalage in the blends. In addition, the second peak of evolution for CO and CO_2 decreased with increase in the propostion of microlage. It is recommended to conduct similar co-pyrolysis studies on a wide range of microlage feedstocks with organic biomass wastes to understand the mechanisms of synergy and the interactions betweeen the major components of each category. Further, it is also recommended to conduct reactor scale studies to decide the optimum conditions, such as mixing ratios, heating rate and final temperature, for co-pyrolysis of similar feedstocks.

Author Contributions

The manuscript was written through contributions of all authors. All authors approved the final version of the manuscript.

Competing interests

The authors declare that they have no competing interests.

Availability of data and materials

Not applicable.

Consent for publication

Authors agreed to publish this article.

Ethics approval and consent to participate

Not applicable.

Funding Sources

The work was supported by National Natural Science Foundation of China (grant number: 51506112), Tsinghua University Initiative Scientific Research Program (grant number: 20161080094), the Guangdong Provincial Key R&D Program (No. 2019B110209001) and the Natural Science Foundation of Guangdong Province (2017A030313438)

Competing interests

The authors declare no competing interests.

References

1. Hosseini, S.E. and M.A. Wahid, *Hydrogen production from renewable and sustainable energy resources: Promising green energy carrier for clean development.* Renewable and Sustainable Energy Reviews, 2016. **57**: p. 850-866.
2. Almendros, A., et al., *Influence of nickel during the thermal degradation of pine cone shell. Study of the environmental implications.* Journal of Cleaner Production, 2018. **183**: p. 403-414.
3. Vuppaladadiyam, A.K., et al., *Solid Waste as a Renewable Source of Energy: A Comparative Study on Thermal and Kinetic Behavior of Three Organic Solid Wastes.* Energy & Fuels, 2019. **33**(5): p. 4378-4388.
4. Vuppaladadiyam, A.K., et al., *Thermal Characteristics and Kinetic Analysis of Woody Biomass Pyrolysis in the Presence of Bifunctional Alkali Metal Ceramics.* ACS Sustainable Chemistry & Engineering, 2019. **7**(1): p. 238-248.
5. Vuppaladadiyam, A.K., et al., *Thermogravimetric and kinetic analysis to discern synergy during the co-pyrolysis of microalgae and swine manure digestate.* Biotechnology for Biofuels, 2019. **12**(1): p. 170.

6. Jeong, K.-H., et al., *CO2-looping in pyrolysis of horse manure using CaCO3.* Journal of Cleaner Production, 2018. **174**: p. 616-624.
7. Vuppaladadiyam, A.K., et al., *Microalgae cultivation and metabolites production: a comprehensive review.* Biofuels, Bioproducts and Biorefining, 2018. **12**(2): p. 304-324.
8. Vuppaladadiyam, A.K., et al., *Sustainability Analysis of Microalgae Production Systems: A Review on Resource with Unexploited High-Value Reserves.* Environmental Science & Technology, 2018. **52**(24): p. 14031-14049.
9. Raheem, A., et al., *A review on sustainable microalgae based biofuel and bioenergy production: Recent developments.* Journal of Cleaner Production, 2018. **181**: p. 42-59.
10. Vuppaladadiyam, A.K., et al., *Impact of Flue Gas Compounds on Microalgae and Mechanisms for Carbon Assimilation and Utilization.* ChemSusChem, 2018. **11**(2): p. 334-355.
11. Liu, G., et al., *Thermal behavior and kinetics of municipal solid waste during pyrolysis and combustion process.* Applied Thermal Engineering, 2016. **98**: p. 400-408.
12. Feng, Q. and Y. Lin, *Integrated processes of anaerobic digestion and pyrolysis for higher bioenergy recovery from lignocellulosic biomass: A brief review.* Renewable and Sustainable Energy Reviews, 2017. **77**: p. 1272-1287.
13. Wu, Z., et al., *Synergistic effects from co-pyrolysis of low-rank coal and model components of microalgae biomass.* Energy Conversion and Management, 2017. **135**: p. 212-225.
14. Zhao, B., et al., *Kinetics evaluation and thermal decomposition characteristics of co-pyrolysis of municipal sewage sludge and hazelnut shell.* Bioresource Technology, 2018. **247**(Supplement C): p. 21-29.
15. Vyazovkin, S., *Some basics en route to isoconversional methodology*, in *Isoconversional Kinetics of Thermally Stimulated Processes.* 2015, Springer. p. 1-25.
16. Chen, L., et al., *Co-pyrolysis kinetics and behaviors of kitchen waste and chlorella vulgaris using thermogravimetric analyzer and fixed bed reactor.* Energy Conversion and Management, 2018. **165**: p. 45-52.
17. Vuppaladadiyam, A.K., et al., *Thermal characteristics and kinetic analysis of woody biomass pyrolysis in presence of bifunctional alkali metal ceramics.* ACS Sustainable Chemistry & Engineering, 2018.
18. Mishra, G. and T. Bhaskar, *Non isothermal model free kinetics for pyrolysis of rice straw.* Bioresource Technology, 2014. **169**: p. 614-621.
19. Friedman, H.L., *Kinetics of thermal degradation of char□forming plastics from thermogravimetry. Application to a phenolic plastic.* Journal of Polymer Science Part C: Polymer Symposia, 1964. **6**(1): p. 183-195.

20. Akahira, T. and T. Sunose, *Method of determining activation deterioration constant of electrical insulating materials.* Res Rep Chiba Inst Technol (Sci Technol), 1971. **16**: p. 22-31.
21. Vyazovkin, S., et al., *ICTAC Kinetics Committee recommendations for performing kinetic computations on thermal analysis data.* Thermochimica acta, 2011. **520**(1-2): p. 1-19.
22. Vyazovkin, S., *Kinetic concepts of thermally stimulated reactions in solids: A view from a historical perspective.* International Reviews in Physical Chemistry, 2000. **19**(1): p. 45-60.
23. Gogoi, M., et al., *Assessments of pyrolysis kinetics and mechanisms of biomass residues using thermogravimetry.* Bioresource Technology Reports, 2018. **4**: p. 40-49.
24. Huang, L., et al., *Influence of catalysts on co-combustion of sewage sludge and water hyacinth blends as determined by TG-MS analysis.* Bioresource technology, 2018. **247**: p. 217-225.
25. Hu, Z., et al., *Characteristics and kinetic studies of Hydrilla verticillata pyrolysis via thermogravimetric analysis.* Bioresource technology, 2015. **194**: p. 364-372.
26. Söyler, N., et al., *Renewable fuels from pyrolysis of Dunaliella tertiolecta: An alternative approach to biochemical conversions of microalgae.* Energy, 2017. **120**: p. 907-914.
27. Zapata, B., et al., *Thermo-kinetics study of orange peel in air.* Journal of thermal analysis and calorimetry, 2009. **98**(1): p. 309-315.
28. Miranda, R., et al., *Pyrolysis of sweet orange (Citrus sinensis) dry peel.* Journal of Analytical and Applied Pyrolysis, 2009. **86**(2): p. 245-251.
29. Zhou, H., et al., *Classification of municipal solid waste components for thermal conversion in waste-to-energy research.* Fuel, 2015. **145**: p. 151-157.
30. Chang, C.-Y., et al., *Pyrolysis kinetics of uncoated printing and writing paper of MSW.* Journal of environmental engineering, 1996. **122**(4): p. 299-305.
31. Sørum, L., M. Grønli, and J. Hustad, *Pyrolysis characteristics and kinetics of municipal solid wastes.* Fuel, 2001. **80**(9): p. 1217-1227.
32. Li, X., et al., *Effect of anaerobic digestion on sequential pyrolysis kinetics of organic solid wastes using thermogravimetric analysis and distributed activation energy model.* Bioresource technology, 2017. **227**: p. 297-307.
33. Gómez, X., et al., *Study of biological stabilization processes of cattle and poultry manure by thermogravimetric analysis and 13C NMR.* Chemosphere, 2007. **68**(10): p. 1889-1897.
34. Peng, X., et al., *Co-pyrolysis between microalgae and textile dyeing sludge by TG–FTIR: Kinetics and products.* Energy Conversion and Management, 2015. **100**: p. 391-402.
35. Azizi, K., M. Keshavarz Moraveji, and H. Abedini Najafabadi, *Simultaneous pyrolysis of microalgae C. vulgaris, wood and polymer: The effect of third component addition.* Bioresource Technology, 2018. **247**: p. 66-72.

36. Zhao, B., et al., *Kinetics evaluation and thermal decomposition characteristics of co-pyrolysis of municipal sewage sludge and hazelnut shell.* Bioresource technology, 2018. **247**: p. 21-29.
37. Marcilla, A., et al., *Characterization of microalgal species through TGA/FTIR analysis: Application to nannochloropsis sp.* Thermochimica Acta, 2009. **484**(1-2): p. 41-47.
38. Shen, D., et al., *Online evolved gas analysis by Thermogravimetric-Mass Spectroscopy for thermal decomposition of biomass and its components under different atmospheres: Part I. Lignin.* Bioresource Technology, 2013. **130**: p. 449-456.
39. Fu, P., et al., *FTIR study of pyrolysis products evolving from typical agricultural residues.* Journal of Analytical and Applied Pyrolysis, 2010. **88**(2): p. 117-123.
40. Giuntoli, J., et al., *Quantitative and kinetic TG-FTIR study of biomass residue pyrolysis: Dry distiller's grains with solubles (DDGS) and chicken manure.* Journal of Analytical and Applied Pyrolysis, 2009. **85**(1): p. 301-312.
41. Chen, Y., J. Duan, and Y.-h. Luo, *Investigation of agricultural residues pyrolysis behavior under inert and oxidative conditions.* Journal of Analytical and Applied Pyrolysis, 2008. **83**(2): p. 165-174.
42. Mallick, D., et al., *Discernment of synergism in pyrolysis of biomass blends using thermogravimetric analysis.* Bioresource Technology, 2018. **261**: p. 294-305.
43. Sanchez-Silva, L., et al., *Pyrolysis, combustion and gasification characteristics of Nannochloropsis gaditana microalgae.* Bioresource technology, 2013. **130**: p. 321-331.
44. Yang, C., et al., *Pyrolysis of microalgae: A critical review.* Fuel Processing Technology, 2019. **186**: p. 53-72.
45. Tang, Z., et al., *Co-pyrolysis of microalgae and plastic: Characteristics and interaction effects.* Bioresource technology, 2019. **274**: p. 145-152.
46. Ansah, E., L. Wang, and A. Shahbazi, *Thermogravimetric and calorimetric characteristics during co-pyrolysis of municipal solid waste components.* Waste Management, 2016. **56**: p. 196-206.
47. Memon, M.Z., et al., *Na2ZrO3 as an Effective Bifunctional Catalyst–Sorbent during Cellulose Pyrolysis.* Industrial & Engineering Chemistry Research, 2017. **56**(12): p. 3223-3230.
48. Chen, C., X. Ma, and Y. He, *Co-pyrolysis characteristics of microalgae Chlorella vulgaris and coal through TGA.* Bioresource technology, 2012. **117**: p. 264-273.
49. Garcia-Maraver, A., et al., *Determination and comparison of combustion kinetics parameters of agricultural biomass from olive trees.* Renewable Energy, 2015. **83**: p. 897-904.

50. Ma, Z., et al., *Determination of pyrolysis characteristics and kinetics of palm kernel shell using TGA–FTIR and model-free integral methods.* Energy Conversion and Management, 2015. **89**: p. 251-259.
51. Fernandez-Lopez, M., et al., *Kinetic analysis of manure pyrolysis and combustion processes.* Waste Management, 2016. **58**: p. 230-240.
52. Ceylan, S. and D. Kazan, *Pyrolysis kinetics and thermal characteristics of microalgae Nannochloropsis oculata and Tetraselmis sp.* Bioresource technology, 2015. **187**: p. 1-5.
53. Gunasee, S.D., et al., *Pyrolysis and combustion of municipal solid wastes: evaluation of synergistic effects using TGA-MS.* Journal of Analytical and Applied Pyrolysis, 2016. **121**: p. 50-61.
54. Xu, X., et al., *Co-pyrolysis characteristics of municipal sewage sludge and hazelnut shell by TG-DTG-MS and residue analysis.* Waste Management, 2017. **62**: p. 91-100.
55. Shuping, Z., et al., *Pyrolysis characteristics and kinetics of the marine microalgae Dunaliella tertiolecta using thermogravimetric analyzer.* Bioresource Technology, 2010. **101**(1): p. 359-365.
56. Chen, W., et al., *Co-pyrolysis of lignocellulosic biomass and microalgae: Products characteristics and interaction effect.* Bioresource Technology, 2017. **245**: p. 860-868.
57. Chen, L., et al., *Co-pyrolysis of chlorella vulgaris and kitchen waste with different additives using TG-FTIR and Py-GC/MS.* Energy Conversion and Management, 2018. **177**: p. 582-591.
58. Azizi, K., M. Keshavarz Moraveji, and H. Abedini Najafabadi, *Characteristics and kinetics study of simultaneous pyrolysis of microalgae Chlorella vulgaris, wood and polypropylene through TGA.* Bioresource Technology, 2017. **243**(Supplement C): p. 481-491.
59. Fermoso, J., et al., *Synergistic effects during the co-pyrolysis and co-gasification of high volatile bituminous coal with microalgae.* Energy Conversion and Management, 2018. **164**: p. 399-409.
60. Li, Z., et al., *Kinetic study of corn straw pyrolysis: Comparison of two different three-pseudocomponent models.* Bioresource Technology, 2008. **99**(16): p. 7616-7622.
61. Zhao, M., et al., *Iso-conversional kinetics of low-lipid micro-algae gasification by air.* Journal of Cleaner Production, 2019. **207**: p. 618-629.
62. Turmanova, S.C., et al., *Non-isothermal degradation kinetics of filled with rise husk ash polypropene composites.* Express Polymer Letters, 2008. **2**(2): p. 133-146.
63. Maia, A.A.D. and L.C. de Morais, *Kinetic parameters of red pepper waste as biomass to solid biofuel.* Bioresource Technology, 2016. **204**: p. 157-163.
64. Gai, C., et al., *Thermogravimetric and kinetic analysis of thermal decomposition characteristics of low-lipid microalgae.* Bioresource Technology, 2013. **150**: p. 139-148.

65. Li, L., et al., *Thermogravimetric and kinetic analysis of Spirulina wastes under nitrogen and air atmospheres.* Bioresource Technology, 2013. **140**: p. 152-157.
66. Mishra, G., J. Kumar, and T. Bhaskar, *Kinetic studies on the pyrolysis of pinewood.* Bioresource Technology, 2015. **182**: p. 282-288.
67. Xu, Y. and B. Chen, *Investigation of thermodynamic parameters in the pyrolysis conversion of biomass and manure to biochars using thermogravimetric analysis.* Bioresource Technology, 2013. **146**: p. 485-493.

Highlights

- Synergism between two dissimilar feedstocks during co-pyrolysis was evaluated.
- Volatiles and extractives in microalgae improved the decomposition pattern of blends.
- Kinetics and gas yields were significantly enhanced.
- Synergistic effect was higher with microalgae -digested biowaste blends than with microalgae-biowaste blends
- Co-pyrolysis can reduce the energy input

Declaration of interests

☒ The authors declare that they have no known competing financial interests or personal relationships that could have appeared to influence the work reported in this paper.

☐The authors declare the following financial interests/personal relationships which may be considered as potential competing interests: